Fundamental Research xxx (xxxx) 1–8

Contents lists available at ScienceDirect

Fundamental Research

journal homepage: www.elsevier.com

Journal Cover Image

Dynamically adjustable topological edge states in thermal diffusion-advection system

Quan Liu [a], Zhaochen Wang [a], Maojin Zeng [b], Hyejeong Kim [c], Wonjoon Choi [c, *], Run Hu [a, d, *]

[a] School of Energy and Power Engineering, Huazhong University of Science and Technology, Wuhan, China
[b] School of Energy and Power Engineering, Xi'an Jiaotong University, Xi'an, China
[c] School of Mechanical Engineering, Korea University, Seoul, Republic of Korea
[d] Department of Applied Physics, Kyung Hee University, Yongin-Si, Gyeonggi-do, Republic of Korea

ARTICLE INFO

Keywords:
Topological edge state
Thermal advection
Thermal metamaterials
Thermal diffusion
Domain wall

ABSTRACT

Topological edge states offer a powerful platform for understanding and manipulating waves, encompassing classical electromagnetic and acoustic wave systems and condensed matter systems. Though topological states have been recently extended from wave to thermal diffusion systems, their realization is still confined to pure thermal conduction, unable to provide a general discussion as lacking access to thermal advection. Here, we attempt to extend the concept of topological edge states from diffusion to diffusion-advection dynamics and reveal the dynamically adjustable counterpart topological edge states. The varying ratios of inter- to intra-coupling advection coefficients can profoundly impact the time evolution of thermal systems, precipitating the emergence of distinct topological states, which cannot happen in a pure conduction system. The diffusion-advection systems are non-Hermitian with eigenvalues consisting of the imaginary component corresponding to diffusion rate and the real component corresponding to advection rate. Upon deriving the governing Hamiltonian of a thermal lattice, we observe the emergence of topological edge states in the gap of bulk states. Additionally, we present a comparative analysis that underscores the unique thermal properties of bulk and edge states enabled by the thermal advection term. Our work paves the way for the exploration of topological states within thermal diffusion-advection systems and potentially provide distinct paradigms for efficient thermal management and thermal protection.

1. Introduction

Thermal metamaterials have witnessed significant progress in manipulating heat flow, ranging from developing capable design methods like transformation thermotics [1,2], scattering cancellation [3], and optimization algorithms [4–6], attempting advanced thermal functionalities like thermal printing [7] and thermal encoding [8], exploring promising applications scenarios like advanced printing circuit boards [9,10], military camouflage [11,12] and illusion devices [13], to revealing the underlying physics like topological edge states, thermal nonreciprocity [3,14,15], thermal nonlinearity [16], coherent perfect absorption [17], etc. Topological physics in heat diffusion is still in its infancy, rather than its counterparts in quantum mechanics and classical wave systems such as electromagnetics, acoustics, mechanics, and condensed matter. The prosperous developments of topological physics in the latter two kinds of systems have refueled the scientific and technical developments significantly, such as topological insulators [18–21] and Weyl semimetals [22], enabling various practical applications beyond the imagination of the last century including topological lasers [23–26] and nanocavity-based sensors [27–29].

Recent advances have further expanded the realm of topological states from wave systems to thermal diffusion systems [30–32] and beyond [33,34]. Diffusive topological edge states have been experimentally and theoretically observed in 1D thermal lattices [35] and 2D thermal networks [36–38], respectively. The emergence of topological edge states in anti-Hermitian systems, characterized by purely thermal diffusion, or in non-Hermitian systems that incorporate advective heat transport, hinges on the introduction of thermal advection [39]. By introducing advection, the diffusion-advection systems are non-Hermitian with eigenvalues consisting of an imaginary part corresponding to diffusion rate and a real part corresponding to advection rate. Moreover, the non-Hermitian skin effect may exist in such systems [40,41]. Yet, the realization of such topological states within thermal diffusion-advection systems has not been achieved thus far.

In this work, we extend the concept of topological phases to the realm of diffusion-advection dynamics, crafting a one-dimensional

* Corresponding author.
E-mail addresses: wojchoi@korea.ac.kr (W. Choi), hurun@hust.edu.cn (R. Hu).

https://doi.org/10.1016/j.fmre.2025.02.001
Received 11 November 2024; Received in revised form 22 January 2025; Accepted 9 February 2025
2667-3258/© 20XX

topological thermal transport model. By conducting thorough theoretical analyses and numerical simulations of the temperature field, we derive the Hamiltonian of the diffusion-advection system. Our findings reveal how the ratio of inter- to intra-coupling advection coefficients, demonstrated as σ, influences the emergence of diverse topological edge states. This investigation could lay the groundwork for the creation of innovative thermal metamaterials, which may have significant implications for topological thermal insulation, enhanced thermal management, and controlled directional heat transfer.

2. One-dimensional thermal topological model

In order to migrate the notion of topological phases from wave systems to diffusion-advection dynamics, we develop a one-dimensional thermal topological model. In this model, both heat diffusion and heat advection with site i_x -1 and i_x +1 exist for any given site i_x. As illustrated in Fig. 1a, we demonstrate the process of deriving the discretized form of the thermal diffusion-advection equation. The temperature at the site i_x depends on the heat transfer process between it and its neighboring sites. The overall model exhibits a unified set of characteristics pertaining to density ρ, heat capacity C_p and the distance between two neighboring sites a. In the process of heat transfer, thermal energy is propelled not merely by pure conduction but also by the directional movement of mass. With thermal advection, the heat flow can be transported into or away from the site at a rate $-\rho C_p v\nabla T$. By introducing the heat advection term, the thermal diffusion equation $\rho C_p \frac{\partial T}{\partial t} = \lambda\nabla^2 T$ evolves into the heat diffusion-advection equation $\rho C_p \frac{\partial T}{\partial t} = \lambda\nabla^2 T - \rho C_p v\nabla T$. In Fig. 1a, λ_{i_x-1,i_x} and v_{i_x-1,i_x} denote the effective thermal conductivity and thermal advection velocity between site i_x -1 and i_x, respectively. In the process of heat transfer in the one-dimensional thermal topological model, the progression of the temperature field can be derived as

$$\begin{aligned}\partial_t T_{i_x} &= -(\rho C)^{-1}\left(q_{i_x,i_{x+1}} - q_{i_{x-1},i_x}\right)/a_0 \\ &\quad - \left[v_{i_x,i_{x+1}}\left(T_{i_{x+1}} - T_{i_x}\right) + v_{i_x-1,i_x}\left(T_{i_x} - T_{i_x-1}\right)\right]/2a_0,\end{aligned} \tag{1}$$

where T_{i_x} is described as the temperature at site i_x, q_{i_x-1,i_x} denotes the heat flux between thermal site i_x -1 and i_x due to thermal diffusion, and the latter term represents the derivative of temperature with respect to time caused by thermal advection. Further derivation of Eq. (1) gives

$$\begin{aligned}\partial_t T_{i_x} &= \left[\left(\lambda_{i_x-1,i_x}\Big/a_0^2\rho C_p\right)T_{i_x-1} + \left(\lambda_{i_x,i_x+1}\Big/a_0^2\rho C_p\right)T_{i_x+1}\right] \\ &\quad - \left(\lambda_{i_x-1,i_x} + \lambda_{i_x,i_x+1}\right)\Big/a_0^2\rho C_p T_{i_x} \\ &\quad + \left[v_{i_x-1,i_x}T_{i_x-1} - v_{i_x,i_x+1}T_{i_x+1} + \left(v_{i_x,i_x+1} - v_{i_x-1,i_x}\right)T_{i_x}\right]/2a_0.\end{aligned} \tag{2}$$

By normalizing thermal diffusion coefficient $D_{i_x-1,i_x} = \lambda_{i_x-1,i_x}\left(a^2\rho C_p\right)^{-1}$ and thermal advection coefficient $V_{i_x-1,i_x} = v_{i_x-1,i_x}(2a)^{-1}$ between thermal site i_x -1 and i_x, the derivative of temperature with respect to time at site i_x can be described as

$$\begin{aligned}\partial_t T_{i_x} &= \left(D_{i_x-1,i_x} + V_{i_x-1,i_x}\right)T_{i_x-1} + \left(D_{i_x,i_x+1} - V_{i_x,i_x+1}\right)T_{i_x+1} \\ &\quad + \left(V_{i_x,i_x+1} - V_{i_x-1,i_x} - D_{i_x-1,i_x} - D_{i_x,i_x+1}\right)T_{i_x}.\end{aligned} \tag{3}$$

Furthermore, we construct a one-dimensional periodic thermal lattice as depicted in Fig. 1b based on the aforementioned model. Each periodic thermal unit cell is constituted by two sites characterized as A and B. We see from Eq. (3) that the progression of the temperature field in the periodic thermal lattice can be delineated as

$$\frac{\partial T_{B,I}}{\partial t} = \left(D_2 + V_2\right)T_{A,I} + \left(D_1 - V_1\right)T_{A,\mathrm{II}} + \left(V_1 - V_2 - D_1 - D_2\right)T_{B,I} \tag{4}$$

$$\frac{\partial T_{A,\mathrm{II}}}{\partial t} = \left(D_1 + V_1\right)T_{B,\mathrm{I}} + \left(D_2 - V_2\right)T_{B,\mathrm{II}} + \left(V_2 - V_1 - D_1 - D_2\right)T_{A,\mathrm{II}} \tag{5}$$

Here $T_{B,\mathrm{I}}$ and $T_{A,\mathrm{II}}$ are designated as the temperature at site B in periodic cell | and site A in periodic cell ‖, respectively. The thermal unit cells are connected by inter-couplings with the normalized thermal diffusion coefficient D_1 and normalized thermal advection coefficient V_1, while within the cellular structure, sites A and B are linked by means of intra-couplings with the normalized thermal diffusion coefficient D_2 and normalized thermal advection coefficient V_2. In the event of N thermal cells, it can be reasonably deduced that these cells are interconnected to constitute a one-dimensional infinite periodic thermal lattice. The governing evolution of the temperature in the periodic thermal lattice takes the form as

$$\frac{\partial T(t)}{\partial t} = -iHT(t) \tag{6}$$

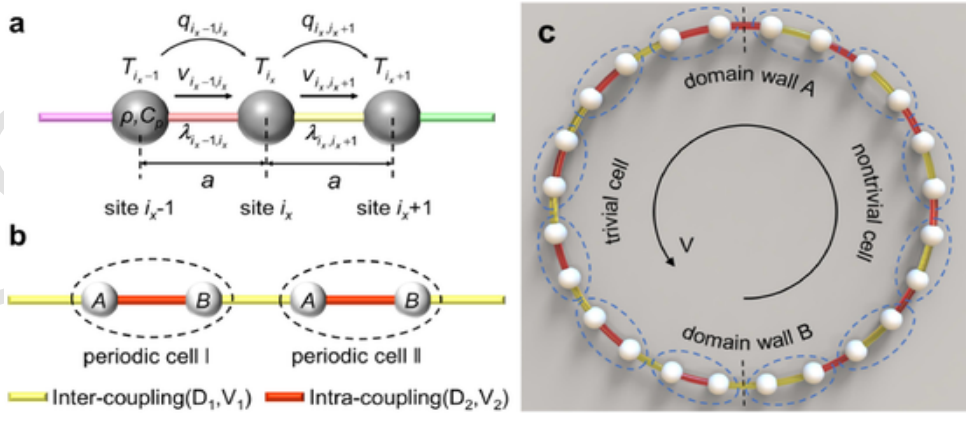

Fig. 1. Schematics of the one-dimensional thermal topological model. (a) Schematic representation of the heat transfer process between site i_x-1 and i_x (i_x and i_x + 1). (b) One dimensional infinite periodic thermal cell. Each unit cell is comprised of sites designated as A and B, respectively. The inter-coupling is denoted by D_1 and V_1, while the intra-coupling is represented by D_2 and V_2. (c) Schematic diagram of the topological thermal lattice structure. In this structure, the trivial cells and the nontrivial cells consisting of different intra-couplings are connected to form a circle, separated by domain wall A and B. The direction of the heat advection velocity between the sites is along the arrow in the figure.

where $T(t) = \left[T_{A,1}(t)\, T_{B,1}(t) \cdots T_{A,N}(t)\, T_{B,N}(t)\right]^T$ represented by the temperature field at a given time t is comprised of elements referring to the on-site temperatures. Inserting N equations analogous to Eqs. (4) and 5 into Eq. (6), the governing Hamiltonian of the periodic thermal lattice can be derived as

$$H_{PTL} = (-i)\begin{bmatrix} D_1+D_2+V_2-V_1 & -(D_1-V_1) & 0 & \cdots & -(D_2 \\ -(D_1+V_1) & D_1+D_2+V_1-V_2 & -(D_2-V_2) & \cdots & 0 \\ 0 & -(D_2+V_2) & D_1+D_2+V_2-V_1 & \cdots & 0 \\ \vdots & \vdots & \vdots & \ddots & \vdots \\ -(D_2-V_2) & 0 & 0 & \cdots & D_1+1 \end{bmatrix}$$

In contrast to the thermal diffusion system, the governing real-space Hamiltonian of the thermal diffusion-advection model is non-Hermitian rather than anti-Hermitian for the dissipative nature of not only heat diffusion but also heat advection. Consequently, the eigenvalue ω consists of the imaginary component corresponding to the thermal diffusion rate and the real component referring to the thermal advection rate.

We consider two types of unit cells separated by domain wall A and B in the topological thermal lattice, as shown in Fig. 1c, in which different unit cells are composed of different intra-couplings. The unit cell with the greater intra-coupling is demonstrated as the trivial cell, whereas the unit cell with the greater inter-coupling is illustrated as the nontrivial cell. The intra-coupling and inter-coupling advection coefficients can be controlled by employing a specific ratio $\sigma = V_1/V_2$. In order to calculate the band structure of the lattice, we apply the Fourier transformation to Eq. (3). The Bloch Hamiltonian of the periodic diffusion-advection thermal lattice in the reciprocal space can be written as

$$H(k) = (-i)\begin{bmatrix} D_1+D_2+V_2-V_1 & -(D_1-V_1)-(D_2-V_2)\,e^{-ik} \\ -(D_1+V_1)-(D_2+V_2)\,e^{ik} & D_1+D_2+V_1-V_2 \end{bmatrix}$$ (8)

In accordance with the elements situated on the antidiagonal of the Bloch Hamiltonian in the reciprocal space, we can ascertain the winding number calculated as

$$\begin{cases} W_1 = \dfrac{1}{2\pi i}\displaystyle\int_{-\pi}^{\pi} dk \frac{d}{dk} \log\left[-(D_1-V_1)-(D_2-V_2)\,e^{-ik}\right] \\ W_2 = \dfrac{1}{2\pi i}\displaystyle\int_{-\pi}^{\pi} dk \frac{d}{dk} \log\left[-(D_1+V_1)-(D_2+V_2)\,e^{ik}\right] \end{cases}$$ (9)

The winding number band structure in the lattice is illustrated in Figs. 2a and b. As σ increases, the two branches of the winding number band coalesce at $\sigma = 1$, and then both W_1 and W_2 vanish to zero. In addition, we illustrated the top view of the winding number band to facilitate observation of the dividing line as W_2 is altered. Subsequently, we demonstrated the eigen spectra in the trivial and nontrivial cells when the thermal diffusion coefficients D_1 and D_2 are fixed equally. It is significant to point out that various outcomes can be observed by adjusting the ratio of the thermal advection coefficients σ, as depicted in Fig. 2c and d. In the case where $\sigma < 1$, the intra-coupling thermal advection coefficient (V_2) is greater than the inter-coupling thermal advection coefficient (V_1). The system is defined as a topological trivial state due to the presence of the trivial cells. As σ is increased from 0 to 1, the peak

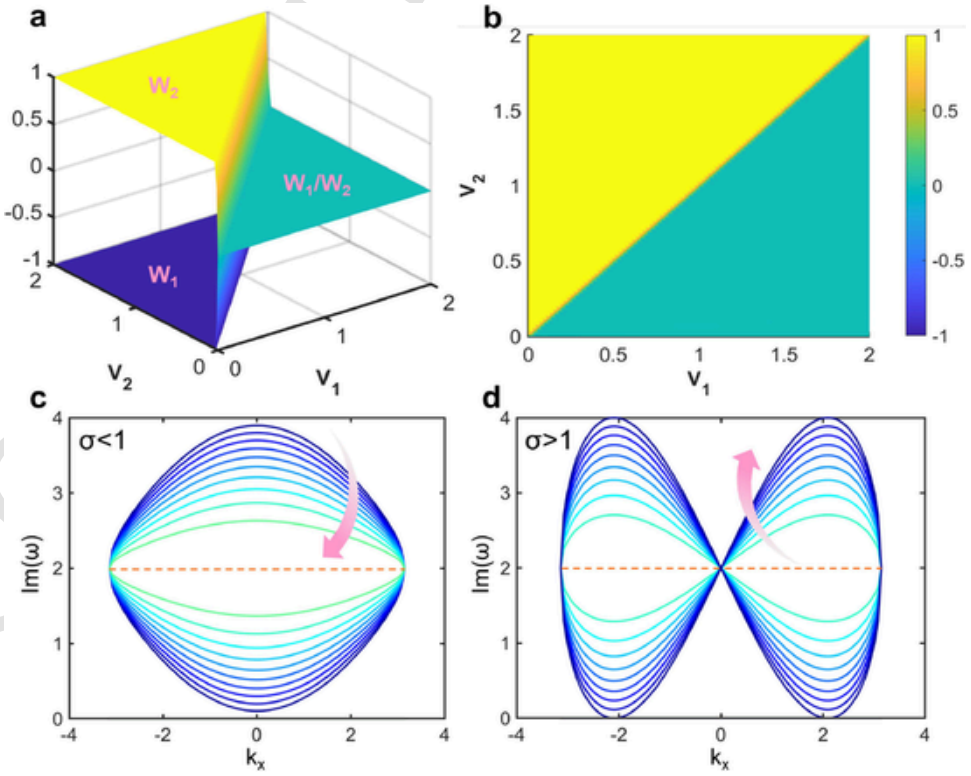

Fig. 2. (a) Winding number band structure in the periodic thermal lattice. W_1 and W_2 assume the same value as zero in the region where V_1 is less than V_2. Conversely, in the region where V_1 is greater than V_2, W_1 and W_2 are split to −1 and 1, respectively. (b) Top view of Fig. 2a. (c, d) Eigen spectra in the trivial and nontrivial cells when the thermal diffusion coefficients D_1 and D_2 are fixed equally. The arrow indicates the direction of increase in σ, and the orange dashed line illustrates that the decay rate remains constant when V_1 is equal to V_2.

value of the energy band at $k = 0$ is observed to decrease, and the colors of the lines in the eigen-spectrum become lighter, until the energy band becomes a horizontal line at $\sigma = 1$ (as the orange dashed line shown in Fig. 2c). Conversely, when $\sigma > 1$, the inter-coupling thermal advection coefficient (V_1) is greater than the intra-coupling thermal advection coefficient (V_2). The system is now demonstrated to be in a topological nontrivial state due to the presence of the nontrivial cells. As σ increases from 1, the peak value of the energy band also increases in a corresponding manner. It is worth noting that a distinct alteration in the energy band occurs, which is characterized by a transition from a single peak to two peaks. The aforementioned alteration serves to indicate the existence of edge states.

3. Observation of thermal topological edge states

In order to observe the thermal topological edge states in the thermal diffusion-advection system, we construct a topological thermal lattice as illustrated in Fig. 1c. Separated by domain wall *A* and *B*, the trivial cells and nontrivial cells are distributed on the left and right side of the lattice, respectively. The direction of the heat advection velocity between the thermal sites is along the arrow in the center of Fig. 1c. A total of 24 thermal sites are arranged in the thermal lattice comprising 6 trivial unit cells located in the left and 6 nontrivial unit cells situated in the right. In accordance with Eqs. (4–6), we can obtain the governing Hamiltonian of the topological thermal lattice in the presence of domain walls as

$$H_{TTL} = (-i)$$

$$\begin{bmatrix} D_1+D_2+V_2-V_1 & \cdots & 0 & 0 & \\ \vdots & \ddots & \vdots & \vdots & \\ 0 & \cdots & D_1+D_2+V_2-V_1 & -(D_1-V_1) & \\ 0 & \cdots & -(D_1+V_1) & D_1+D_2+V_1-V_1 & \\ 0 & \cdots & 0 & -(D_1+V_1) & D_1 \\ \vdots & \ddots & \vdots & \vdots & \\ 0 & \cdots & 0 & 0 & \\ -(D_2-V_2) & \cdots & 0 & 0 & \end{bmatrix}$$

By solving the eigenvalues of the real-space Hamiltonian, the thermal diffusion rate spectrum of the periodic thermal lattice and topological thermal lattice have been delineated as depicted in Fig. 3. When the thermal advection coefficients V_1 and V_2 are both set to zero, the thermal diffusion-advection system is degraded into a thermal diffusion system, reflecting the purely dissipative nature of heat conduction. Then, its corresponding eigenvalue ω is purely imaginary and correlates with the thermal diffusion rate. From the eigen spectra, it can be observed that only bulk states exist in the periodic thermal lattice. In contrast, two distinct edge states emerge within the decay-rate gap of bulk modes in the topological thermal lattice, as indicated in Fig. 3a. Edge state | and ‖ can be identified by means of the corresponding eigenvectors. Edge state | exhibits a symmetric mode profile at domain wall *A*, whereas edge state ‖ demonstrates an asymmetric mode profile at domain wall *B,* as denoted in Fig. 3b. The eigenvectors of edge state | are mainly distributed in the middle, whereas those of edge state ‖ are mainly distributed at the position of two boundaries. The distinction between the two edge states is attributed to the disparate thermal diffusion coefficients that pertain to the regions surrounding the two domain walls. In the case where neither V_1 nor V_2 is zero and $\sigma = V_1/V_2 > 1$, the governing Hamiltonian is no longer anti-Hermitian since heat transfer includes heat diffusion and heat advection in the thermal diffusion-advection model. Thus, the eigenvalue ω consists of the imaginary part denoted as thermal diffusion rate and the real part indicated as thermal advection rate. The thermal diffusion rate is employed as the horizontal axis, whereas the thermal advection rate is utilized as the vertical axis (presented in Fig. 3c). Similar to the case of thermal diffusion system, edge states do not exist in the periodic thermal lattice, while the topological thermal lattice exhibits edge state | and ‖ inside the thermal diffusion rate gap of bulk states in the thermal diffusion-advection system. Theoretical derivations reveal that once the number of sites reaches a critical threshold, the bulk states evolve into two elliptical rings, as indicated by the dashed lines in Fig. 3c. Concurrently, the edge states are found to reside within the band gap that separates these two elliptical rings. It is worth mentioning that edge state | and ‖ both indicate asymmetric mode profiles at domains *A* and *B*, resulting from the unidirectionality of the heat advection velocity. At domain wall *A*, the thermal site and its adjacent sites are connected with greater thermal advection coefficients. Consequently, the heat transfer of edge state | is more rapid. At domain wall *B*, the site and its adjacent sites are connected with less thermal advection coefficients. As a result, the heat of edge state ‖ is transferred more slowly. The direction of thermal advection aligns with the direction of ascending thermal sites, so we can observe a higher concentration of eigenvectors on the right side of the peak compared to the left side in Fig. 3d.

Furthermore, in theoretical calculation, the eigen spectra of the periodic thermal lattice and topological thermal lattice are depicted in Fig. 4. In the periodic thermal lattice as indicated in Figs. 4a and b, the thermal diffusion rate spectrum and the thermal advection rate spectrum only exhibit bulk states, regardless of velocity ratio $\sigma > 1$ or $\sigma < 1$. In other words, no edge states appear in the system if the thermal unit cells are arranged periodically. When $\sigma = 1$, the thermal diffusion rates and the thermal advection rates are almost uniformly distributed. In the case where $\sigma < 1$, the lattice consists of trivial unit cells. As σ increases, the thermal diffusion rate band merges and the band gap narrows, demonstrating an increase in the ratio of inter- to intra-coupling advection coefficients, whereas the thermal advection rate band remains almost unchanged. When $\sigma > 1$, the lattice is comprised of nontrivial unit cells. Conversely, there hasn't been much change to the thermal diffusion rate band as σ increases. Besides, the amplitude of the thermal advection rate band increases, indicating that the thermal advection coefficient is increased in the meantime. Additionally, in the topological thermal lattice as illustrated in Figs. 4c and d, the eigen spectra show similar trends to the spectra in the periodic thermal lattice. As σ increases, denoting an increased ratio of inter- to intra-coupling advection coefficients, the thermal diffusion rate band also becomes progressively narrower, while the thermal advection rate band tends to be widened. When $\sigma < 1$, there are not too many changes in the thermal diffusion and advection rate bands, which indicates that edge states do not occur in the system. Conversely, when $\sigma > 1$, edge states are presented in the topological thermal lattice. The positions of the edge states remain unchanged in the middle of the thermal diffusion rate band as the bandwidth narrows, demonstrating that the position of the edge state in the thermal diffusion lattice is independent of the ratio of inter- to intra-coupling advection coefficients σ, as denoted in Fig.4c. Besides, as σ increases, the amplitude of the thermal advection rate band becomes larger and edge states are distributed at the position of two boundaries of the thermal advection rate band, as indicated by their corresponding eigenvectors. Consequently, it can be observed that the distinction between edge states marked with red dots and bulk states marked with black dots is getting more pronounced as σ increases in Fig.4d, resulting from the increased thermal advection coefficient. The eigenvectors corresponding to the edge states are almost distributed at the position of two boundaries, exhibiting identical positions with the eigenvalues. The change in σ increases the difference between the thermal advection coefficients V_1 and V_2, which leads to an increase in thermal advection rate, i.e., the real part of the eigenvalue ω of the edge states in the system. These differences in mode profiles between the periodic thermal lattice and the topological thermal lattice emphasize the crucial influence of the arrangement of the thermal unit cells in our one-dimensional thermal topological model.

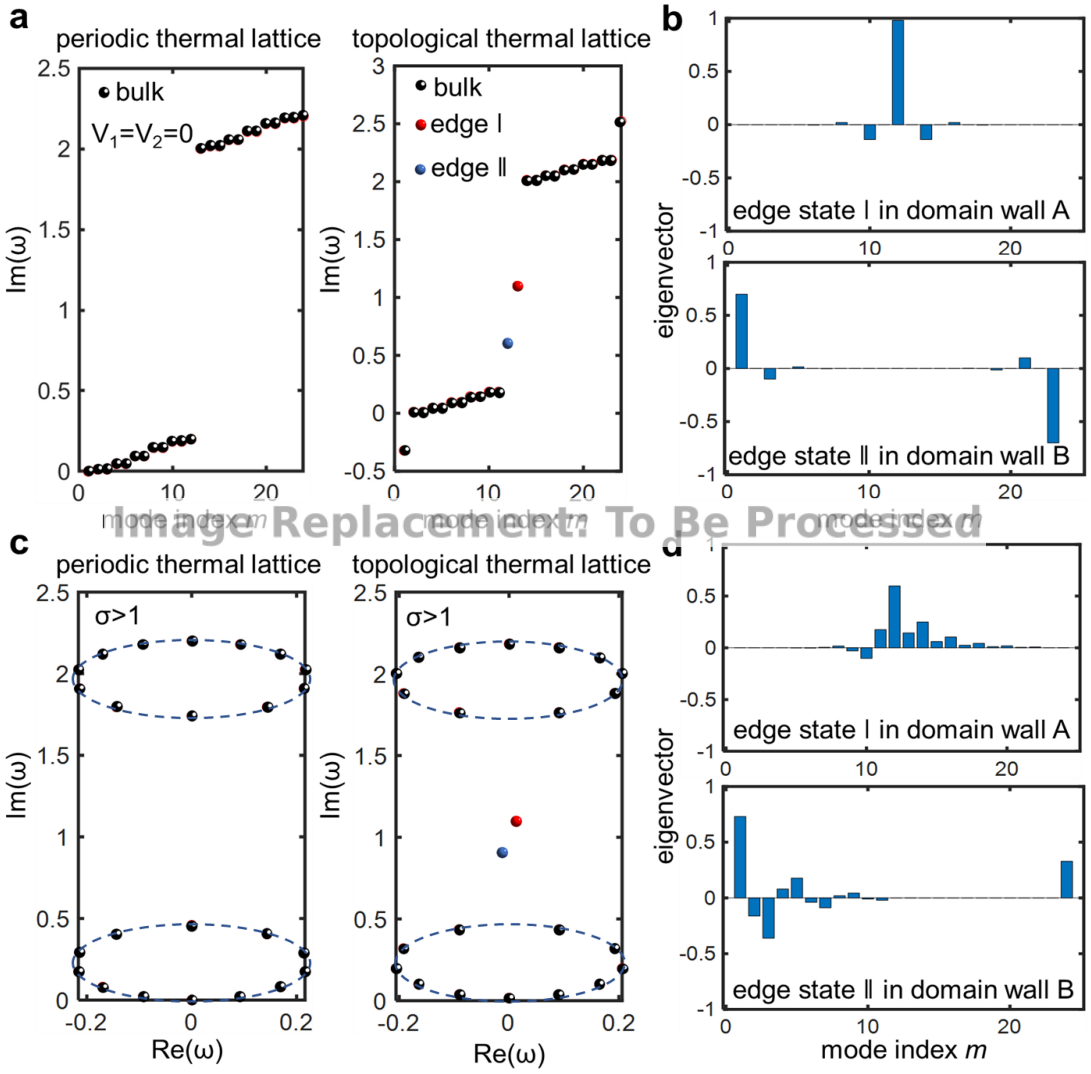

Fig. 3. Observation of topological edge states in the topological thermal lattice. (a) Decay-rate bands and mode profiles in the periodic thermal lattice and topological thermal lattice in the absence of thermal advection. (b, d) Comparison of eigenvectors under edge state | in domain wall *A* and edge state ‖ in domain wall *B* in the presence and absence of thermal advection. (c) Decay-rate bands and mode profiles in the presence of thermal advection.

Due to the appearance of these edge states, the on-site temperature at the domain wall decreases at a different rate, compared to that in the bulk state. In addition to theoretical calculations, numerical finite-element method simulations using COMSOL Multiphysics are also conducted to further validate this phenomenon. We develop a topological thermal lattice to form a circle as indicated in Fig. 1c and the material in simulation is aluminum 6063-T83 (thermal conductivity $\lambda = 201 W/$ (m •K), density $\rho = 2700 kg/m^3$ and heat capacity $C_p = 900 J/$ (kg •K)) in COMSOL Multiphysics. The radii of the thermal site and topological lattice are set as 0.06 m and 1.02 m, respectively. Thus, the distance between two thermal sites can be calculated as 0.267 m. We set 293 K as the room temperature and 400 K as the initial temperature on the heated thermal site. In addition, the ratio of inter- to intra-coupling advection coefficients σ is set as 9 to demonstrate edge states and we regulate σ by adjusting the thermal advection velocity. The velocity of thermal advection can be achieved by driving fluid through an electromagnetic actuation module on each site, which has been proven feasible [39]. We assign the initial temperature to the thermal sites corresponding to edge state |, edge state ‖ and bulk states respectively, and monitor their on-site temperature evolution with time. The temperature is normalized with $T_{norm} = \ln[(T-T_r)/(T_i-T_r)]$, where T_r is the room temperature and T_i is the initial temperature of heated thermal site. Consequently, the normalized temperature evolutions for edge state |, edge state ‖ and bulk states in the topological thermal lattice are illustrated in Fig.5a. In theoretical terms, the eigenvalue of the system is anticipated to diminish exponentially as time progresses, with the decay rate corresponding to the imaginary component of the eigenvalue. At edge state | in domain wall *A*, the thermal site and its neighboring sites are associated with larger thermal advection coefficients. Therefore, the heat dissipation of edge state | is more rapid and the normalized temperature decreases at a faster rate. At edge state ‖ in domain wall *B*, the site and its neighboring sites are associated with lower thermal advection coefficients. As a result, the heat of edge state ‖ is dissipated more slowly and the normalized temperature decreases at a slower rate.

The temperature field distribution of different states is demonstrated in Figs. 5b–d. After 100 s, the highest temperature of edge state | has descended to 339.4 K, while the highest temperature of bulk state is 342.3 K and that of edge state ‖ is still 342.9 K. It is obvious that the temperature of edge state | exhibits the most rapid decline, followed by bulk state and edge state ‖, and the temperature reduction at edge state ‖ proceeds at a pace that is marginally slower compared to the bulk state. The outcomes from both numerical simulations and theoretical

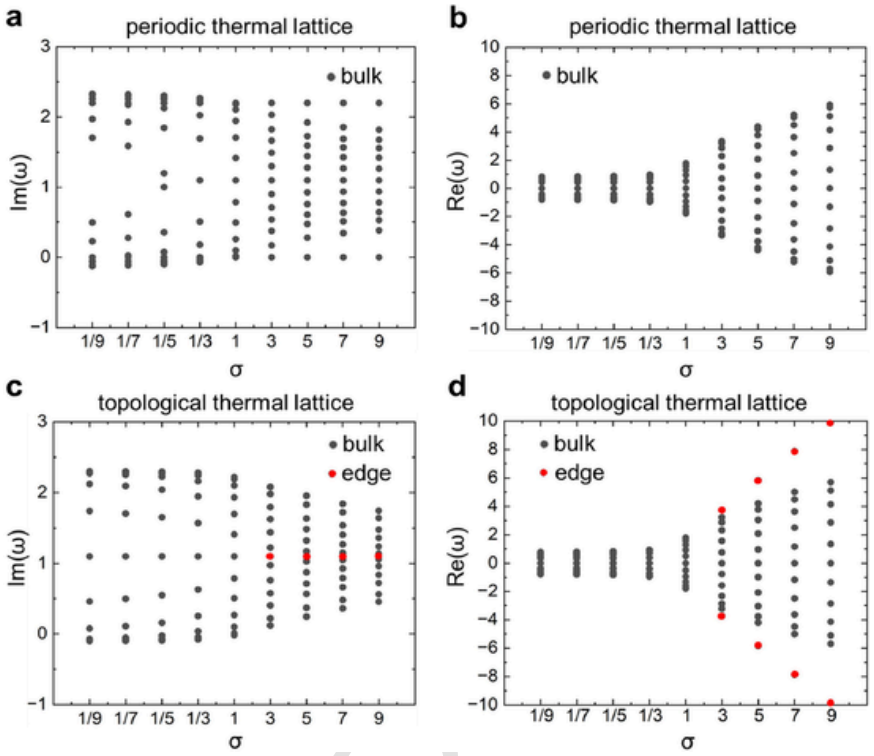

Fig. 4. Eigen spectra of periodic thermal lattice and topological thermal lattice structure. (a, b) Decay rate and eigenfrequency (imaginary and real part) spectrum of the periodic thermal lattice. (c, d) Mode profiles and eigen spectrum of the topological thermal lattice.

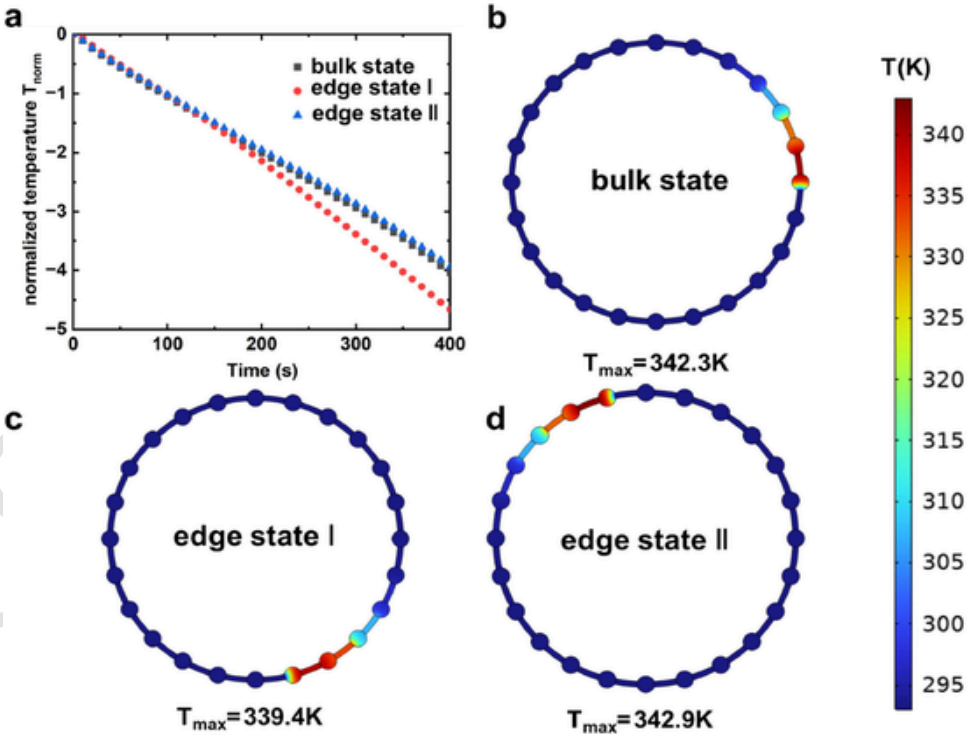

Fig. 5. (a) Time evolution of normalized temperature for the bulk state, edge state | and edge state ‖ under topological thermal lattice structure. (b-d) Temperature field distribution of the bulk state, edge state | and edge state ‖ in the topological thermal lattice (t = 100 s).

calculations agree well, thereby confirming the precision of our model in depicting the thermal field of the actual heat transfer system.

4. Conclusion

In summary, we integrated thermal advection into purely diffusive heat-transfer systems to investigate the dynamically adjustable topological edge states in the one-dimensional thermal lattice via theoretical analysis and simulation validation, revealing two topological edge states | and ‖. Upon deriving the Hamiltonian of the thermal lattice, we discerned the onset of topological edge states within the gap of bulk states. Notably, the edge state | exhibits a swiftly diminishing and localized temperature profile under the domain-wall sphere excitation. We demonstrated how the ratio of inter- to intra-coupling advection coefficients σ impacts the emergence of various topological edge states. Our results may stimulate further exploration of topological states of matter in diffusion-advection systems beyond 1D system. Moreover, these insights are anticipated to enrich our comprehension of topological thermal protection and temperature management, promising to facilitate the development of innovative thermal systems with topologically guaranteed robustness.

Uncited Reference

[31]

Declaration of competing interest

The authors declare that they have no conflicts of interest in this work.

Acknowledgements

The authors acknowledge the financial support from National Key R & D Project from Ministry of Science and Technology of China (2022YFA1203100, 2024YFB4104701), National Natural Science Foundation of China (52422603, 92463311, 52076087), Interdisciplinary Research Program of HUST (5003120094), and Natural Science Foundation of Hubei Province (2023AFA072).

References

[1] C.Z. Fan, Y. Gao, J.P. Huang, Shaped graded materials with an apparent negative thermal conductivity, Appl. Phys. Lett. 92 (2008) 251907.
[2] R. Hu, S. Zhou, Y. Li, et al., Illusion thermotics, Adv. Mater 30 (2018) 1707237.
[3] R. Ju, P.-C. Cao, D. Wang, et al., Nonreciprocal heat circulation metadevices, Adv. Mater. 36 (2024) 2309835.
[4] Z. Zhu, X. Ren, W. Sha, et al., Inverse design of rotating metadevice for adaptive thermal cloaking, Int. J. Heat Mass Tran. 176 (2021) 121417.
[5] Z. Zhu, Z. Wang, T. Liu, et al., Arbitrary-shape transformation multiphysics cloak by topology optimization, Int. J. Heat Mass Transfer 222 (2024) 125205.
[6] Z. Wang, Z. Zhu, T. Liu, Inverse design of thermal metamaterials with holey engineering strategy, J. Appl. Phys. 132 (2022) 145102.
[7] R. Hu, S. Huang, M. Wang, et al., Encrypted thermal printing with regionalization transformation, Adv. Mater. 31 (2019) 1807849.
[8] R. Hu, S. Huang, M. Wang, et al., Binary thermal encoding by energy shielding and harvesting units, Phys. Rev. Appl. 10 (2018) 054032.
[9] C. Zhao, J. Liu, B. Li, et al., Multiscale construction of bifunctional electrocatalysts for long-lifespan rechargeable zinc–Air batteries, Adv. Funct. Mater. 30 (2020) 2003619.
[10] S. Imhof, C. Berger, F. Bayer, et al., Topolectrical-circuit realization of topological corner modes, Nat. Phys. 14 (2018) 925–929.
[11] R. Hu, W. Xi, Y. Liu, et al., Thermal camouflaging metamaterials, Mater. Today 45 (2021) 120–141.
[12] W. Xi, Y. Lee, S. Yu, et al., Ultrahigh-efficient material informatics inverse design of thermal metamaterials for visible-infrared-compatible camouflage, Nat. Commun. 14 (2023) 4694.
[13] T. Liu, Z. Wang, Z. Zhu, et al., General three-dimensional thermal illusion metamaterials, Chin. Phys. B 33 (2024) 044401.
[14] M. Lei, P. Jin, Y. Zhou, et al., Reconfigurable, zero-energy, and wide-temperature loss-assisted thermal nonreciprocal metamaterials, Proc. Natl. Acad. Sci. 121 (2024) e2410041121.
[15] Y. Li, J. Li, M. Qi, et al., Diffusive nonreciprocity and thermal diode, Phys. Rev. B 103 (2021) 014307.
[16] Y. Zhou, T. Ding, G. Xu, et al., Sustainable heat harvesting via thermal nonlinearity, Nat. Rev. Phys. (2024).
[17] Y. Li, M. Qi, J. Li, et al., Heat transfer control using a thermal analogue of coherent perfect absorption, Nat. Commun. 13 (2022) 2683.
[18] M.Z. Hasan, C.L. Kane, Colloquium: topological insulators, Rev. Mod. Phys. 82 (2010) 3045.
[19] X.-L. Qi, S.-C. Zhang, Topological insulators and superconductors, Rev. Mod. Phys. 83 (2011) 1057.
[20] C.-Z. Chang, J. Zhang, X. Feng, et al., Experimental observation of the quantum anomalous hall effect in a magnetic topological insulator, Science 340 (2013) 167–170.
[21] K. He, Y. Wang, Q.-K. Xue, Topological materials: quantum anomalous hall system, Annu. Rev. Condens. Matter Phys 9 (2018) 329–344.
[22] X. Wan, A.M. Turner, A. Vishwanath, et al., Topological semimetal and fermi-arc surface states in the electronic structure of pyrochlore iridates, Phys. Rev. B 83 (2011) 205101.
[23] B. Bahari, A. Ndao, F. Vallini, et al., Nonreciprocal lasing in topological cavities of arbitrary geometries, Science 358 (2017) 636–640.
[24] M.A. Bandres, S. Wittek, G. Harari, et al., Topological insulator laser: experiments, Science 359 (2018) eaar4005.
[25] G. Harari, M.A. Bandres, Y. Lumer, et al., Topological insulator laser: theory, Science 359 (2018) eaar4003.
[26] Y. Zeng, U. Chattopadhyay, B. Zhu, et al., Electrically pumped topological laser with valley edge modes, Nature 578 (2020) 246–250.
[27] H.-R. Kim, M.-S. Hwang, D. Smirnova, et al., Multipolar lasing modes from topological corner states, Nat. Commun. 11 (2020) 5758.
[28] Y. Ota, F. Liu, R. Katsumi, et al., Photonic crystal nanocavity based on a topological corner state, Optica 6 (2019) 786.
[29] W. Zhang, X. Xie, H. Hao, et al., Low-threshold topological nanolasers based on the second-order corner state, Light Sci. Appl. 9 (2020) 109.
[30] Z. Liu, P. Jin, M. Lei, et al., Topological thermal transport, Nat. Rev. Phys. 6 (2024) 554–565.
[31] H. Hu, S. Han, Y. Yang, et al., Observation of topological edge states in thermal diffusion, Adv. Mater. 34 (2022) 2202257.
[32] H. Wu, H. Hu, X. Wang, et al., Higher-order topological states in thermal diffusion, Adv. Mater. 35 (2023) 2210825.
[33] L. Xu, G. Dai, Wang G, et al., Geometric phase and bilayer cloak in macroscopic particle-diffusion systems, Phys. Rev. E 102 (2020) 032140.
[34] Z. Liu, J. Huang, Topological plasma transport from a diffusion view, Chin. Phys. Lett. 40 (2023) 110305.
[35] M. Qi, D. Wang, P. Cao, et al., Geometric phase and localized heat diffusion, Adv. Mater. 34 (2022) 2202241.
[36] Z. Wang, T. Liu, Z. Zhu, et al., Periodicity alters topological states in thermal diffusion system, Int. J. Heat Mass Tran. 235 (2024) 126182.
[37] Z. Liu, P.-C. Cao, L. Xu, et al., Higher-order topological In-bulk corner State in pure diffusion systems, Phys. Rev. Lett. 132 (2024) 176302.
[38] G. Xu, X. Zhou, S. Yang, et al., Observation of bulk quadrupole in topological heat transport, Nat. Commun. 14 (2023) 3252.
[39] S. Yang, G. Xu, X. Zhou, et al., Hierarchical bound states in heat transport, Proc. Natl. Acad. Sci. 121 (2024) e2412031121.
[40] K. Zhang, Z. Yang, C. Fang, Universal non-Hermitian skin effect in two and higher dimensions, Nat. Commun. 13 (2022) 2496.
[41] Z. Li, L. Wang, X. Wang, et al., Observation of dynamic non-Hermitian skin effects, Nat. Commun. 15 (2024) 6544.

Quan Liu received his B.S. degree in 2023 from Huazhong University of Science and Technology and majored in energy and power engineering. Currently, he is a master student at Huazhong University of Science and Technology under the supervision of Professor Run Hu. His research interests focus on thermal nonreciprocity, convective thermal metamaterials and topological thermal transport.

Wonjoon Choi received the B.S. degree in mechanical and aerospace engineering from Seoul National University, Korea, in 2003, and the Ph.D. degree in mechanical engineering (ME) from the Massachusetts Institute of Technology (MIT), Massachusetts, USA, in 2012. In 2012, he was the postdoctoral researcher in chemical engineering from MIT, and joined Korea University, Korea as a faculty, the same year. He is currently a professor in school of mechanical engineering, Korea University. His research interests include multiscale thermal-fluidic transports, materials and devices for energy conversion and storage, and multifunctional metamaterials.

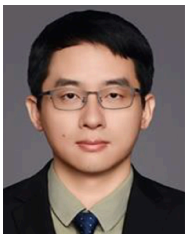

Run Hu (BRID: 05579.00.70695) received his bachelor and Ph.D. degrees from Huazhong University of Science and Technology in 2010 and 2015, respectively. He has been a visiting scholar at Purdue University in the United States and a JSPS special researcher at the University of Tokyo in Japan. Currently, he is a professor in school of energy and power engineering, Huazhong University of Science and Technology. His main research interests include heat and mass transfer, thermal superstructure materials and functional devices, and thermal management of optoelectronic devices.